frontiers | Frontiers in Marine Science

TYPE Original Research
PUBLISHED 02 July 2024
DOI 10.3389/fmars.2024.1285429

OPEN ACCESS

EDITED BY
Lyne Morissette,
M – Expertise Marine, Canada

REVIEWED BY
Natascha Wosnick,
Federal University of Paraná, Brazil
Peter Gausmann,
Ruhr University Bochum, Germany

*CORRESPONDENCE
M. G. Meekan
m.meekan@gmail.com

RECEIVED 30 August 2023
ACCEPTED 08 May 2024
PUBLISHED 02 July 2024

CITATION
Meekan MG, Thompson F, Brooks K, Matsumoto R, Murakumo K, Lester E, Dove A and Hopper B (2024) Internal organs and body tissues of free-swimming whale sharks (*Rhincodon typus*) imaged using underwater ultrasound.
Front. Mar. Sci. 11:1285429.
doi: 10.3389/fmars.2024.1285429

Internal organs and body tissues of free-swimming whale sharks (*Rhincodon typus*) imaged using underwater ultrasound

M. G. Meekan[1*], F. Thompson[2], K. Brooks[3], R. Matsumoto[4], K. Murakumo[4], E. Lester[1], A. Dove[5] and B. Hopper[6]

[1]Oceans Institute, University of Western Australia, Perth, WA, Australia, [2]Mira Mar Veterinary Hospital, Albany, WA, Australia, [3]Australian Institute of Marine Science, University of Western Australia, Perth, WA, Australia, [4]Okinawa Churashima Foundation, Okinawa Churaumi Aquarium, Motobu, Okinawa, Japan, [5]Research and Conservation Department, Georgia Aquarium, Atlanta, GA, United States, [6]Animalius, Perth, WA, Australia

Ultrasound imaging can be used as an effective tool to measure the reproductive status and condition of sharks. This usually requires restraint of the subject, which is not feasible in the wild when the target species is of conservation concern and very large, as is the case for whale sharks. Our study invoked a behavioral response in free-swimming whale sharks that allowed snorkelers to image internal organs and structures using a submersible ultrasound scanner linked to an iPhone in an underwater housing. We were able to reliably locate and monitor the heart and other internal organs inside the body cavity, structures inside the head, and image skin and muscle in the dorsal surface of the sharks. The technique is evaluated as a means for assessing the condition and reproductive status of free-swimming whale sharks.

KEYWORDS

elasmobranchs, chondrichthyes, condition, reproduction, underwater ultrasound, brain, heart, intestine

Introduction

As a filter feeder that often resides at the surface of tropical oceans, whale sharks face major challenges in the Anthropocene due to increasing pollution of marine systems by plastic debris (Fossi et al., 2017; Germanov et al., 2018, Germanov et al., 2019; Yong et al., 2021; Rowat et al., 2021) and the threat of damage and scarring due to collision with vessels (Speed et al., 2008; Rowat et al., 2021; Womersley et al., 2022). The degree to which such threats might affect the feeding and ultimately the condition of these sharks is unknown. In part, this is because our understanding of anatomy, reproduction and factors driving body condition in whale sharks is very limited (Pierce et al., 2021b). Knowledge of the reproductive cycle is restricted to the observation of a single pregnant female that was captured in a targeted fishery in the waters off

Taiwan (Joung et al., 1996). For these reasons, techniques to measure body condition and reproductive status through imaging of internal organs would aid in management and conservation planning of the species.

Ultrasound provides an effective means to image the internal organs (Lai et al., 2004) and assess the reproductive status of elasmobranchs [see (Penfold and Wyffels, 2019) for review]. This non-lethal technique has been used where sharks are held in aquaria, however the procedure is often invasive since imaging may require restraint and/or anesthesia of the animal unless it is sampled *post-mortem*. In the field, sampling of live sharks usually requires capture using hook and line (Hoyos-Padilla et al., 2023). The stress involved in capture and restraint can result in significant chance of mortality and in some cases, spontaneous abortion by pregnant females (Godin et al., 2012).

Although ultrasound techniques are useful for species that can be easily captured and are robust to the procedure, the method is less suitable for species such as whale sharks, which grow to immense sizes [up to 18 m in total length; (Mcclain et al., 2015)]. Because of their Endangered status (International Union for the Conservation of Nature Red List; (Pierce and Norman, 2016) they are protected from capture or harm by legislation in many countries (Pierce et al., 2021a) and where they occur close to coasts and are thus accessible to researchers, they are often the subject of valuable ecotourism industries that are supported by management plans that strictly regulate interactions with the species (Mau, 2008; Huveneers et al., 2017; Reynolds et al., 2024).

In this study, our aim was to determine if we could use ultrasound imagery in a minimally invasive approach to accurately and reliably identify internal organs within the body cavity and tissues in the head and on the dorsal surface of free-swimming sharks. Ultimately, our goal was to evaluate the potential of the use of the ultrasound technique for the assessment of body and reproductive condition of free-swimming whale sharks.

Methods

Study site and sampling technique

Ultrasound images were collected over the first two weeks in May of 2020 and 2021 during an annual program to monitor the whale shark aggregation at Ningaloo Reef, Western Australia. This timing coincided with the seasonal peak in numbers of the animals, which aggregate at Ningaloo between March and July (Meekan et al., 2006). Hotspots of shark numbers are found around Norwegian Bay and Point Cloates and were the focus of our study (see Figure 1 in (Dugal et al., 2022). To sample sharks, light planes were used to locate animals on the surface and their positions were communicated to the sampling boat so that snorkelers could enter the water to swim with the shark. The divers photographed the left and right flanks for photo-identification of individuals (Meekan et al., 2006; Speed et al., 2007), recorded the shark using underwater stereo-video for later measurement of body size (Sequeira et al., 2016) and sampled tissue biopsies for genetic studies (Meenakshisundaram et al., 2021; Dugal et al., 2022). Parasitic copepods were then collected from the shark for genetic and isotopic studies (Meekan et al., 2017, Meekan et al., 2022; Osorio et al., 2023). These copepods were scraped from the lips and leading edges of the pectoral fins and the ventral surface towards the

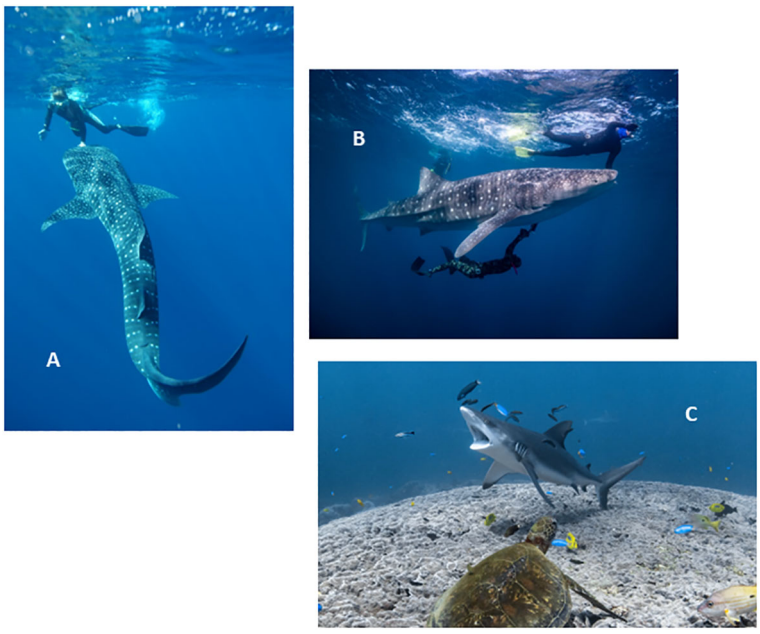

FIGURE 1
(A). Whale shark in vertical "cleaning posture" as copepod parasites are removed from the mouth of the shark by a snorkeler. Photo credit: Rob Harcourt. **(B)**. Ultrasound scanner in use on underside of shark. Photo credit Andre Rerekura. **(C)**. Grey reef shark (*Carcharhinus amblyrhynchos*) in cleaning posture at a reef cleaning station on Ningaloo Reef WA. Photo credit: Ningaloo Marine Interactions.

mouth using a plastic knife by a snorkeler swimming alongside the unrestrained shark (Meekan et al., 2017). The process of removing the parasites often invoked a behavioural response from the shark where it stopped forward motion and hung vertically in the water column, which we assume was a "cleaning posture" (Figure 1A). With the shark in this position, the underwater ultrasound scanner (see Supplementary Information) was able to be applied to either the dorsal or ventral surface of the shark during snorkeling (Figure 1B). The tail-down posture of the shark resembled the behavior of reef sharks at cleaning stations on coral reefs when parasites are removed by cleaning fishes (Figure 1C). If the shark did not slow and assume the cleaning position, or if it dived, no sonography was attempted.

Ultrasound imaging

We used a commercially available wireless livestock ultrasound scanner (Duo-Scan: Go Plus livestock ultrasound scanner | IMV imaging (imv-imaging.com)) to image the internal tissues of whale sharks. The Duo Scan is a freestanding unit that transmits the sonogram through its own internal wireless to a phone/tablet application (BCF Go Scan App). Here, we linked the scanner to an Apple iPhone in a waterproof housing. Both were housed on a custom mount with a GoPro Hero 4 (See Supplementary Figure 1). Synchronizing of the frame captures from ultrasound video in the iPhone allowed the GoPro to simultaneously record the position of the ultrasound transducer on the body of the whale shark (Supplementary Figure 1). Although there are other underwater ultrasound units commercially available, this product was selected as was a compact, free-standing device that transmitted images directly to an iPhone, allowing the operator to simultaneously scan and visualize organs with both instruments mounted on the same frame while free diving. It also provided the best compromise in terms of cost and image quality. Settings and specifications for the Duo Scan are given in Supplementary Information.

The operator commenced recording of the ultrasound and GoPro prior to entry to the water for each shark, and the entire sampling period from entry to the return to the boat was recorded in one sequence. These video files were later exported from the iPhone as MP4 files and reviewed in standard Windows and Mac video playback software. Where measurements were required, videos were imported into open-source software designed for motion analysis (www.kinovea.org) and the images calibrated with the displayed scale for the acquisition of linear measurements. Medical standard DICOM image format is not available with this equipment.

The ultrasound transducer is a convex linear array with a frequency of 3–6 MHz. The maximum depth (24 cm) and penetration mode (lowest frequency) were selected after gain settings were optimized in trials that varied the frequency of the scan, depth of penetration and resolution of the resulting image. This gain was then set prior to sampling, as there was no ability to easily adjust settings on the iPhone in the housing once in the water.

Scanning technique involved predominantly sagittal plane imaging (see Supplementary Figure 2) with a combination of slow sliding and periodic lifting and re-positioning the transducer on the skin of the shark. External landmarks were identified to help orientate the images and determine likely anatomy on the image (Supplementary Figure 3). On the underside of the shark (ventral surface), these were the pectoral line with is an imagined transverse line joining the front edge of the pectoral fins, and the longitudinal midline crease (Supplementary Figure 3).

The broad, flat dorsal surface of the head provided ample access for sonography. Images were acquired in the sagittal and transverse plane (Supplementary Figure 2), sliding from cranial (front) to caudal (back) and left to right. Sagittal images were acquired slightly to the left and right of midline and further laterally. Midline images had poor contact between the skin and transducer due to a midline ridge, so were not acquired after the first day. The dorsal (back) musculature was imaged at points alongside and in the region of the dorsal fin.

Results

In total, 13 individual sharks were sampled using ultrasound in 2020 and 37 in 2021. Nearly all of these were juvenile male sharks ranging in length from 3.5–8 m (see Supplementary Table 1). Below we describe and illustrate the sonographic anatomy of the body tissues and organs imaged during our field work. Ultrasound videos from which the images shown in Figures 2–11 were captured are provided in Supplementary Information.

Abdomen

The ventral abdominal wall structure of all sharks was of fine linear fibers oriented in a longitudinal plane, with thin, hyperechoic transverse bands running the thickness of the wall at intervals along the ventral body (intervals varied, some 4.5 cm apart). This corresponded to the hypaxial musculature separated into myotomes. The ventral abdominal wall varied in thickness. In

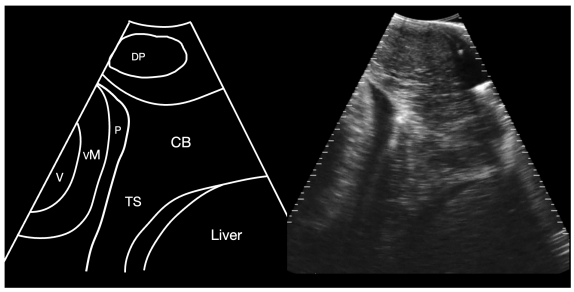

FIGURE 2
Schematic diagram (left) and corresponding sagittal sonogram (right) acquired at the pectoral line, showing the transverse septum. CB Coracoid bar; P Pericardial fluid; TS Transverse septum; VM ventricular myocardium; V Ventricular lumen. See Supplementary Video S1.

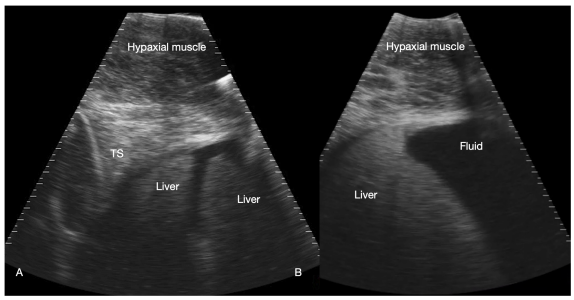

FIGURE 3
Liver. Sagittal sonograms of shark 31 at the pectoral line **(A)** and caudal to the pectoral line **(B)** showing the transverse septum (TS), liver and peritoneal fluid. Image displayed depth 21 cm, left of the image is cranial. See Supplementary Video S2.

Shark 34 (male, 4.5 m length) it ranged from 5 cm in the midline over the gallbladder (just caudal to the pectoral girdle), to 9 cm in the parasagittal region at the same level.

The cranial margin of the midline crease and the pectoral line were used as landmarks to commence sonographic evaluation of the sharks, and at this level the cranial extent of the abdominal cavity was identified, bounded by the transverse septum, identified as a broad shelf of moderately echoic tissue that separated the abdominal cavity caudally from the pericardial space cranially (Figure 2). The base of this septum was confluent with the coracoid bar, identified as a broadening of the ventral septum in the body wall. Also identified at this level was the depressor pectoralis muscle, imaged in transverse and forming an ovoid hypoechoic structure in the hypaxial musculature.

Structures within the abdomen that were consistently identified were the liver, gallbladder, bile duct and stomach (Figures 2–6). Structures not identified were the spleen, spiral valve, kidneys, or reproductive organs.

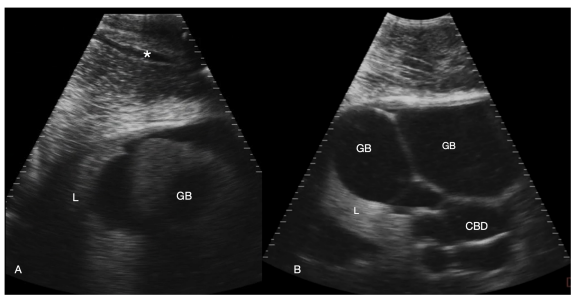

FIGURE 4
Gallbladder and bile duct. Sagittal sonograms caudal to the pectoral line, display depth 21 cm. Images are displayed with cranial to the left. **(A)** Right parasagittal sonogram Shark 31. In the abdominal wall a tubular anechoic vein is visible (*). The gallbladder is small and imaged poorly adjacent to the liver. **(B)** Midline sagittal sonogram, just caudal to the pectoral line in Shark 34. The gallbladder is distended and folded in the near field and the common bile duct and possibly portal vessels in folded tubes in the far field. Some liver parenchyma is to the left of the image (cranial). See Supplementary Video S3.

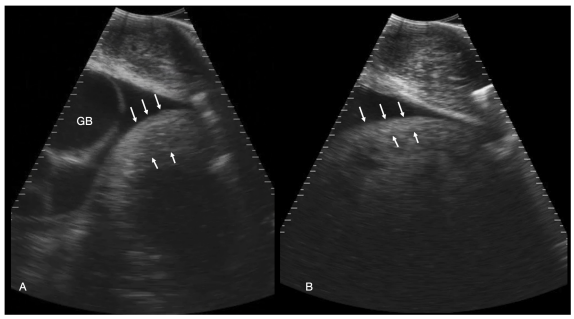

FIGURE 5
Stomach. **(A)** Left parasagittal sonogram caudal to the liver and gallbladder in shark 34. The stomach is small and the wall ~ 2.7 cm thick (between the white arrows). The contents are anechoic fluid. The gallbladder (GB) is distended. **(B)** Left parasagittal sonogram caudal to the liver in shark 31. The stomach wall (between the arrows) is thinner than in A, measuring ~ 2 cm in thickness. The gastric contents are echoic and shadowing, consistent with feeding. See Supplementary Video S4.

Liver

The liver was recognized by its characteristic shape and sonographic appearance of finely granular parenchymal texture that was generally hyperechoic, becoming hyperattenuating in some individuals. This is consistent with hepatic sonographic appearance in other species with increasing lipid content causing attenuation of the ultrasound beam (Mattoon et al., 2020). The liver was visible from the pectoral girdle to a point caudal to the pelvic fins. The entire liver was not imaged in each animal due to limitations of access and compliance. At the cranial extent there were curved, convex margins that conformed to the transverse septum surface (Figure 3). The lobes were separated by a moderate volume of nearly anechoic peritoneal fluid. In the cranial portion, the lobar margins were triangular in transverse section, with slightly

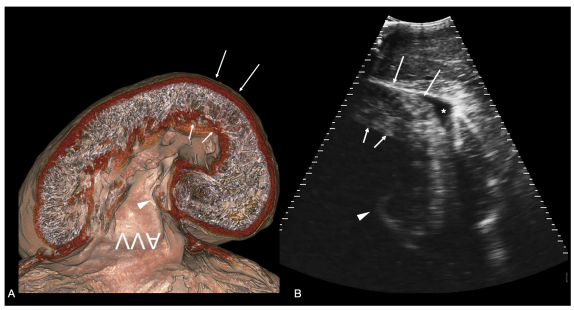

FIGURE 6
Atrioventricular valve. **(A)** Sagittal CT image of plastinated whale shark heart specimen reproduced from (Hirasaki et al., 2018) showing the ventricular myocardium and atrioventricular valve (AVV) - image inverted to correspond to the sonographic image. **(B)** Sagittal sonogram of the heart of whale shark 31 acquired on the ventral midline cranial to the pectoral line. The ventricular myocardium (arrows) and posterior leaflet of the atrioventricular valve (arrowhead) are clearly differentiated. In the near field (top of the image) is the hypaxial muscle of the ventral body wall, and a small volume of anechoic fluid surrounds the myocardium (marked *) within the pericardial space. The displayed depth is 21cm. See Supplementary Video S5.

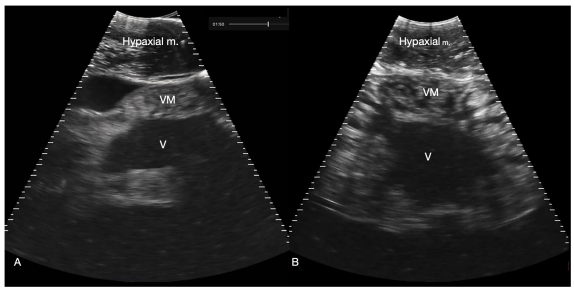

FIGURE 7
Myocardium. **(A)** Sagittal ventral sonogram cranial to the pectoral line showing the conus arteriosus, shark 31 (cranial oriented to the left of the image). **(B)** Sagittal ventral sonogram just cranial to the pectoral line showing the ventricular myocardium, shark 31. Note the striated appearance with alternating hyperechoic (white) and hypochoic (dark) bands within the myocardium. M: Ventricular myocardium, V: Ventricular lumen. See Supplementary Video S6A, B.

rounded margins. In the mid and caudal abdomen, the liver was positioned in the dorsolateral cavity and was seen as a strap-like, smoothly marginated structure with some occasional internal, tubular anechoic structures (venous sinus likely but not confirmed). The gallbladder was identified on and just to the right of midline, immediately caudal to the pectoral girdle (Figure 4). It was a large, elongated oval structure with a thin wall and anechoic fluid contents. When distended (up to 7.5 cm diameter), it folded on itself and was separated from the adjacent liver by anechoic peritoneal fluid. Dorsal and caudal to the gallbladder a broad tubular structure 2 – 3.5 cm in diameter was identified, coursing caudally in the sagittal plane, consistent with the common bile duct. Dorsal to the gallbladder was a cluster of thin-walled, fluid filled tubes. These may be tortuous bile duct or hepatic portal vascular structures, or a combination of both.

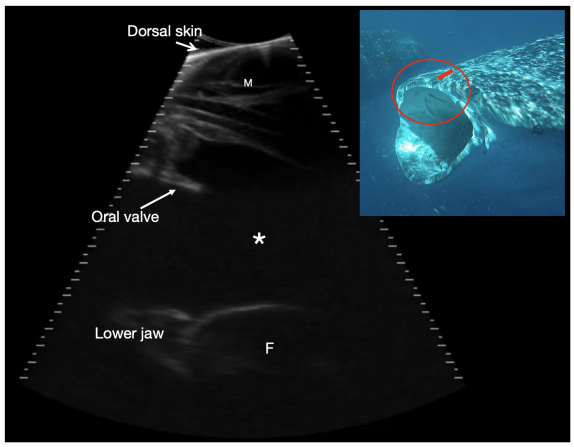

FIGURE 8
Rostral orobranchial chamber. Parasagittal sonogram, cranial to the left. The skin edge is imaged in the near field (top of image) due to incomplete transducer contact, and there is maxillary muscle (M) deep to the skin. The orobranchial chamber is filled with anechoic fluid (*). It is bounded dorsally by oral mucosa and projecting into the lumen is a caudally projecting shelf corresponding to an oral valve (see insert image). The ventral interfaces (at the bottom of the image) correspond to the ventral surface of the orobranchial chamber with a portion of filter pad (F) imaged towards the caudal (right) side of the image, with its broadly convex surface. The mouth is closed and the chamber height ~ 9 cm. Photograph insert shows the approximate transducer position in (red rectangle) and region imaged circled in red, on a shark with mouth in the open position to better show the oral valves. The sonogram is of a shark with mouth closed. See video S7. Whale shark photo credit Lucy Armstrong.

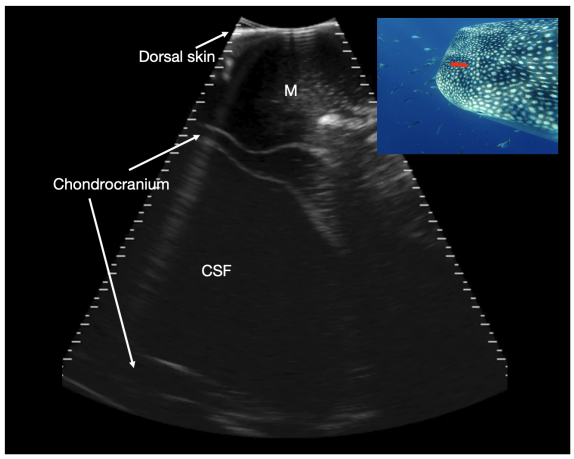

FIGURE 9
Parasagittal neurocranium. Slightly paramedian sagittal sonogram of mid dorsal calvarium. The image is oriented with rostral to the left of the image. A large, fluid filled cavity is present deep to the dorsal musculature and surrounded by chondrocranium (marked CSF), at a depth between 7 and 11 cm. This is thought to correspond to a large cavity that contains cerebrospinal fluid (CSF), extending rostrally from the brain into the rostral dorsal head. Photograph insert shows dorsal view of a whale shark head and approximate transducer position in red. Photo credit Lucy Armstrong.

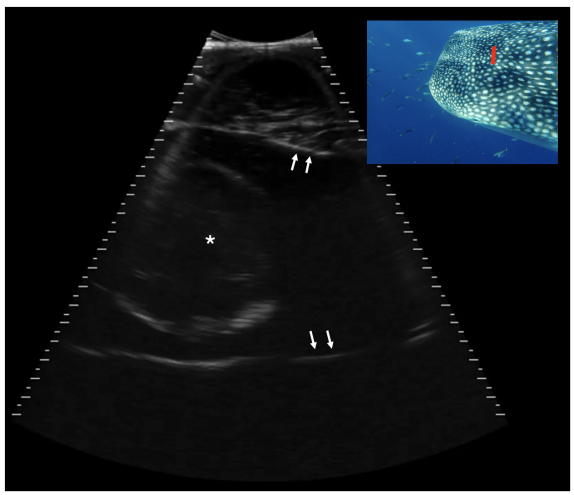

FIGURE 10
Transverse caudal neurocranium, slightly right of midline, Shark 78. The white arrows indicate the internal surface of the calvarial chamber, filled with anechoic fluid. Centrally in the chamber there is a circular structure 8.1 cm in height with a thin, hyperechoic (bright) capsule and some mixed internal echoes. This structure may represent the brain. Displayed depth 21 cm, left is to the right of the image. See video S8. Photograph insert shows dorsal view of a whale shark head and approximate transducer position in red. Photo credit Lucy Armstrong.

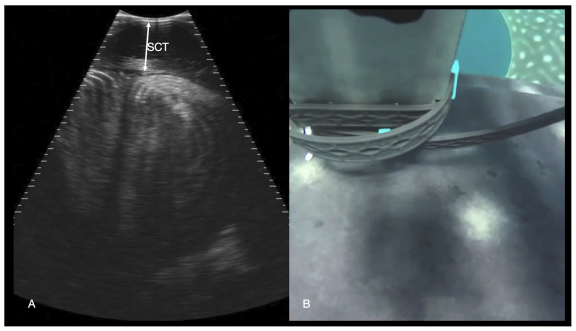

FIGURE 11
Epaxial musculature. **(A)** Transverse right paramedian sonogram of the dorsal myomeres just caudal to the pectoral fins. The subcutaneous connective tissue (SCT) depth is marked with an arrow. Displayed depth is 21 cm, left of the animal is to the left of the image. See video S9. **(B)** Synchronized GoPro image of the transducer position for the sonogram in **(A)** The left pectoral fin is visible in the top right-hand corner of the image, and the midline spinal ridge visible just in front of the transducer.

Stomach

The stomach was consistently visualized immediately caudal to the gallbladder, at midline and slightly left of midline. It was a thick-walled, ovoid structure that varied in size and content from a small amount of anechoic fluid, to larger amounts of amorphous, hyperechoic material surrounded by anechoic fluid (Figure 5). Wall thickness varied from 0.5 cm (shark 29) to 2.7 cm (shark 34). The dorsal extent of the stomach was not reliably determined in most sharks due to a combination of shadowing contents or beam attenuation at depth.

Pericardium

The caudal rigid pericardium was confluent with the transverse septum that divided the pericardial cavity from the abdominal cavity at the level of the pectoral girdle. The transverse septum extended dorsally from the coracoid bar which was recognized as a broadening of the tissue at the base of the septum. (Figure 3). The dorsal and cranial extent of the pericardium was beyond the field of view of the sonographic image. Within the pericardium was a variable volume of anechoic fluid surrounding the heart.

Heart

The heart was readily identified cranial to the pectoral line, at midline. The ventricular wall thickness was ~4 cm during systole and ~2.5 cm in diastole. The atrioventricular valve was identified throughout its excursion (Figure 6). The thin-walled atrium was mostly beyond the extent of beam penetration, only partially visible beyond the valve annulus, and the sinus venosus was not visualized. Cranial to the ventricle, also on the midline, the conus arteriosus was identified as a funnel-shaped, muscular tube oriented in the sagittal plane (Figure 7). Sonographic anatomy was confirmed by correlating sonograms with published CT images of whale shark heart plastinated specimens (Hirasaki et al., 2018). When multiple heart contractions were observed a heart rate was calculated, and these ranged from 12 – 16 beats per minute.

Head

At the rostral extent of the head, the maxilla was visible as a thin, shadowing structure with a narrow convex margin. The ultrasound beam penetrated the dorsal tissues of the cranium and the water within the orobranchial chamber permitted identification of the caudally projecting oral valves and the lower jaw and filter pads (Figure 8). Images acquired further from midline showed striated rectangular structures consistent with teeth.

Just caudal to the maxilla, the neurocranium expanded and surrounded a broad cavity filled with anechoic, or occasionally slightly echoic, cerebrospinal fluid (CSF) (Figure 9). In some individuals, the echoes within this structure's contents were observed to be motile, confirming it to be fluid. In two individuals (Sharks 78 and 91) transverse sequences through the caudal neurocranium (at the caudal margin of the dorsal indentation in the head), revealed a circular structure on midline, measuring approximately 80–85 mm in diameter. This showed a thin, hyperechoic rim and slightly heterogeneous, internal echoes (Figure 10). The location within CSF in the caudal head suggests this represents the rostral portion of the brain. Images acquired more caudally on the dorsal calvarium showed extensive, complex musculature.

Dorsal body

The paraspinal musculature was imaged at several points along the dorsum (caudal to the gills, parasagittal caudal to the dorsal fin and along the mid lateral back). In the transverse plane the roughly rectangular myomeres were identified with concentric hyperechoic lamellae (Figure 11). The thickness of the connective tissue deep to the skin was readily distinguished on the images but appeared to vary according to the anatomic site and as the position of image acquisition was not standardized in this initial study, connective tissue thickness was not recorded.

Discussion

Our results show that the internal organs and body tissues of free-swimming whale sharks can be imaged using an underwater ultrasound scanner that was operated without the use of SCUBA equipment. Our approach should be applicable to any location

where whale sharks gather at the surface in coastal waters and are amenable to the removal of external parasites. At Ningaloo Reef, the technique requires that observers have adequate free diving skills to maintain a position on the shark for sufficient time to locate "landmarks" externally and internally within the body cavity so that different organs can be imaged. Restrictions placed on interactions of swimmers with whale sharks at Ningaloo Reef by management agencies (see: https://www.dpaw.wa.gov.au/plants-and-animals/animals/whale-sharks?showall=&start=2%20) prevent the use of motorized swimming apparatus and SCUBA gear, so the ability of a researcher to slow the shark and evoke a cleaning posture are critical to success of data acquisition.

The use of ultrasound to provide interpretable images relies on adjustment of the transducer position, angle, pressure, and motion in real time by the operator. There are significant challenges using ultrasound in an environment where there is very limited control over the target animal, the environment and the ultrasound equipment. The visibility and size of the image on the screen of the phone was also restricted. This required some investment of time and effort in familiarizing the operator with the equipment and was another reason why the ability to locate organs such as the heart that were easily recognizable and could be used as landmarks within the body was a critical first step. Once this was achieved, we found that we could obtain high quality images of other internal structures of the animal.

The procedure also relied on the shark remaining cooperative and ceasing or slowing forward motion for time sufficient to locate organs. We did not attempt to scan every whale shark we encountered in the study. Limits on breath-hold meant that only those sharks swimming at the water surface provided suitable subjects for sampling and some individuals descended to depth immediately when snorkelers entered the water. For this reason, only around a third of the encountered sharks were scanned. Once a structure was within the ultrasound field of view, static images or long pauses in the transducer movement were helpful to produce optimal detail in images. Small movements of translation or rotation aided structure characterization but were very difficult to control. Translational (sliding) sequences were helpful for describing the relationship of structures to one another, but typically provided poor image detail due to artifacts of motion of the sensor.

Validation of the identity of anatomical structures seen in a sonogram usually requires comparisons with *post-mortem* dissections or cross-sectional imaging using computed tomography (CT) or magnetic resonance imaging (MRI) of the target species. Although *post-mortem* CT images of the whale shark heart (Hirasaki et al., 2018) and MR images of the brain (Yopak and Lawrence, 2009) are available, the use of these cross sectional imaging techniques for *in situ* organ anatomy was clearly not feasible due to the size of the animals, and lack of specimens available for *post mortem* imaging. Whale sharks strand occasionally on beaches in southern Africa (Wosnick et al., 2022) and more rarely in Australia (Speed et al., 2009) and other localities (Sampaio et al., 2018; Whitehead et al., 2019), but access to these sharks is complicated by the very unpredictable timing of strandings and the sometimes remote coastlines where it occurs. Whale sharks are also taken by fisheries in Asia, although in many cases access to these sharks can be complicated by the legal status of these industries (Nijman, 2023). Reproductive and some general sonographic anatomy has been reported in several other captive and wild species of sharks, mostly using restraint (Walsh et al., 1993; Carrier et al., 2003; Daly et al., 2007; Tomita et al., 2019), and there is a comprehensive description of anatomy of the banded houndshark (*Triakis scyllium*) imaged by CT and MRI (Kim et al., 2021), however there is no published data on the abdominal anatomy of the whale shark. For these reasons, we relied on the experience of staff at the Okinawa and Georgia aquariums who had performed ultrasound and *post-mortem* examinations on whale sharks, and on knowledge of comparative sonographic anatomy in other elasmobranchs and mammals to identify internal structures imaged by the ultrasound.

The body condition of sharks is often assessed using data on the lipid content of the liver. This is an elongated organ that occupies much of the length of the abdomen in sharks and has a very characteristic sonographic appearance, not dissimilar to that of mammals (Mattoon et al., 2020). It is a relatively homogeneous, granular, solid parenchymal organ with moderate echogenicity. Increasing lipid content within hepatocytes increases the echogenicity (brightness) of the liver, although this is not reliably quantified with ultrasound as interpretation of echogenicity is subjective. We found this to be the case in whale sharks as we recorded no obvious differences in ultrasound images of the liver of sharks across a range of body sizes. In other species, quantification of hepatic echogenicity requires the use of a calibrated reference phantom and sophisticated ultrasound systems not available in small portable units (Andre et al., 2014). For these reasons, coupled with the challenges of obtaining tissue samples for validation, attempting to quantify hepatic lipid content using sonographic features was found to be impractical, as is the case for other non-invasive techniques such as MR spectroscopy, quantitative CT and ultrasound elastography (Goceri et al., 2016). However, measurement of condition of whale sharks may still be possible using sonography of the dorsal skin and musculature. Biopsy sampling of whale sharks on the dorsal surface has shown that the connective tissue between the layer of dermal denticles on the outer surface of the skin and the muscle layer below can vary substantially in density and thickness among individual sharks (Meekan unpubl. data). We found that we could clearly image the depth of this connective tissue along the back of the shark, but that the skin thickness in an individual varied with the location on the shark. In livestock industries, ultrasound evaluation of subcutaneous back fat depth is well established as a tool to predict carcass fat composition, body condition scoring and degree of muscle marbling. This information is used to direct

management practices and genetic selection of breeding stock (Tait, 2016). Development of a standardized technique to replicate ultrasound sampling along the dorsal surface of whale sharks, in combination with accurate morphometric measurements using techniques such as stereo video (Sequeira et al., 2016) may provide a means to explore links between body shape and skin depth to provide a measure of condition in whale sharks that does not rely on hepatic lipids.

Since the aggregation of whale sharks at Ningaloo Reef is dominated by juvenile males (typically 80% of encounters) with the remainder of individuals mostly small, immature females (Meekan et al., 2006), these animals provided little information on reproductive status. Additionally, the sexual maturity of males can be determined externally by the size and morphology of the claspers present next to the pelvic fins (Matsumoto et al., 2019). However, as we were able to image internal organs easily and quickly, the technique could be applicable for use to assess the reproductive status of female sharks in aggregation sites where adults are present and sex ratios are more balanced between males and females [e.g., Gulf of California; (Ketchum et al., 2013)] or are dominated by females [e.g., Galapagos Islands; (Acuña-Marrero et al., 2014)]. Indeed, ultrasound studies of females in the latter locality are ongoing (Pierce et al., 2021b). Recent work on bull sharks (*Carcharhinus leucas*) at a provisioning site in Mexico confirms that small, submersible ultrasound units can provide useful information on the reproductive status of large, free-swimming sharks (Hoyos-Padilla et al., 2023). Additionally, underwater ultrasound has now been used to document the reproductive status of free-swimming manta rays at cleaning stations on reefs in the Maldives (Froman et al., 2023).

We could reliably image the heart of a whale shark and monitor the activity of this organ. This revealed a heartbeat of around 12 - 16 beats per minute, a rate comparable to that of whale sharks imaged by ultrasound in aquaria (7- 18 bpm, K. Murakomo unpubl. data). Our sonograms captured the action of the ventricular contraction and atrioventricular valve motion (see video S5). It is not known whether heart rate variability would be a reliable indicator of health or stress in this species, however sonography may provide data for future research into this metric.

Despite this success, several organs remain to be imaged by ultrasound within the body cavity. We were unable to locate the spiral valve, which has a very characteristic structure of tightly spiraling plates in a tapering cylinder along the caudal ventral abdominal wall. It is possible this was more dorsally or laterally located and remained beyond the depth of penetration of the ultrasound scanner (24 cm) or may have been more caudal than we attempted to sample (only one scan proceeded further caudally than the pelvic fins). This was still surprising, as the spiral colon is such a prominent structure on the ultrasound images of other shark species. Similarly, the spleen was not identified, however it has a very similar sonographic signature to the liver (in other species) so may have been misidentified on our relatively short sequences of video. Other organs such as the kidneys and gonads were also not reliably identified, possibly due to limited image acquisition in the more caudal portion of the body cavity.

Future research will explore links between ultrasound imaging of the dorsal surface and skin tissues and body morphometry to derive indices for body condition of whale sharks. In addition to ultrasound scanning, the ability to arrest the forward motion of whale sharks by invoking a cleaning response may provide other opportunities for sampling. Parasite collections can provide information on the DNA (Meekan et al., 2017) and recent diet of the whale shark host (Osorio et al., 2023). It may also provide opportunities to collect samples of the shark microbiome and eDNA (Dugal et al., 2022) and to attach, adjust or remove biologging and satellite tags from fins.

Data availability statement

The original contributions presented in the study are included in the article/Supplementary Material. Further inquiries can be directed to the corresponding author.

Ethics statement

The animal study was approved by Animal Ethics Office of Research The University of Western Australia 35 Stirling Highway, Perth WA 6009. The study was conducted in accordance with the local legislation and institutional requirements.

Author contributions

MM: Conceptualization, Formal analysis, Funding acquisition, Investigation, Methodology, Project administration, Resources, Writing – original draft, Writing – review & editing. FT: Conceptualization, Investigation, Writing – review & editing. KB: Data curation, Investigation, Methodology, Project administration, Writing – review & editing. RM: Formal analysis, Writing – review & editing. KM: Formal analysis, Writing – review & editing. EL: Investigation, Writing – review & editing. AD: Formal analysis, Investigation, Writing – review & editing. BH: Conceptualization, Formal analysis, Investigation, Methodology, Writing – original draft, Writing – review & editing.

Funding

The author(s) declare financial support was received for the research, authorship, and/or publication of this article. Santos Ltd provided funding for field work. The funder was not involved in the study design, collection, analysis, interpretation of data, the writing of this article or the decision to submit it for publication. The Georgia Aquarium provided salary support for AD to participate in the study.

Acknowledgments

We thank Terry Maxwell and the crew of the Osso Blue and numerous volunteers and students for their aid in field work.

Conflict of interest

The authors declare that the research was conducted in the absence of any commercial or financial relationships that could be construed as a potential conflict of interest.

The author(s) declared that they were an editorial board member of Frontiers, at the time of submission. This had no impact on the peer review process and the final decision.

Publisher's note

Supplementary material

The Supplementary Material for this article can be found online at: https://www.frontiersin.org/articles/10.3389/fmars.2024.1285429/full#supplementary-material

References

Acuña-Marrero, D., Jiménez, J., Smith, F., Doherty, P. F. Jr., Hearn, A., Green, J. R., et al. (2014). Whale shark (*Rhincodon typus*) seasonal presence, residence time and habitat use at Darwin Island, Galapagos Marine Reserve. *PLoS One* 9, e115946. doi: 10.1371/journal.pone.0115946

Andre, M. P., Han, A., Heba, E., Hooker, J., Loomba, R., Sirlin, C. B., et al. (2014). "Accurate diagnosis of nonalcoholic fatty liver disease in human participants via quantitative ultrasound," in *2014 IEEE International Ultrasonics Symposium*. (Piscataway NJ USA: IEEE) 2375–2377.

Carrier, J. C., Murru, F. L., Walsh, M. T., and Pratt, H. L. Jr. (2003). Assessing reproductive potential and gestation in nurse sharks (*Ginglymostoma cirratum*) using ultrasonography and endoscopy: an example of bridging the gap between field research and captive studies. *Zoo Biology: Published affiliation Am. Zoo Aquarium Assoc.* 22, 179–187. doi: 10.1002/200.10088

Daly, J., Gunn, I., Kirby, N., Jones, R., and Galloway, D. (2007). Ultrasound examination and behavior scoring of captive broadnose sevengill sharks, *Notorynchus cepedianus* (Peron 1807). *Zoo Biology: Published affiliation Am. Zoo Aquarium Assoc.* 26, 383–395. doi: 10.1002/200.20155

Dugal, L., Thomas, L., Jensen, M. R., Sigsgaard, E. E., Simpson, T., Jarman, S., et al. (2022). Individual haplotyping of whale sharks from seawater environmental DNA. *Mol. Ecol. Resour.* 22, 56–65. doi: 10.1111/1755-0998.13451

Fossi, M. C., Baini, M., Panti, C., Galli, M., Jiménez, B., Muñoz-Arnanz, J., et al. (2017). Are whale sharks exposed to persistent organic pollutants and plastic pollution in the Gulf of California (Mexico)? First ecotoxicological investigation using skin biopsies. *Comp. Biochem. Physiol. Part C: Toxicol. Pharmacol.* 199, 48–58. doi: 10.1016/j.cbpc.2017.03.002

Froman, N., Genain, M. A., Stevens, G. M., and Pearce, G. P. (2023). Use of underwater contactless ultrasonography to elucidate the internal anatomy and reproductive activity of manta and devil rays (family: Mobulidae). *J. Fish Biol.* 103, 305–323. doi: 10.1111/jfb.15423

Germanov, E. S., Marshall, A. D., Bejder, L., Fossi, M. C., and Loneragan, N. R. (2018). Microplastics: no small problem for filter-feeding megafauna. *Trends Ecol. Evol.* 33, 227–232. doi: 10.1016/j.tree.2018.01.005

Germanov, E. S., Marshall, A. D., Hendrawan, I. G., Admiraal, R., Rohner, C. A., Argeswara, J., et al. (2019). Microplastics on the menu: plastics pollute Indonesian manta ray and whale shark feeding grounds. *Front. Mar. Sci.* 6, 487857. doi: 10.3389/fmars.2019.00679

Goceri, E., Shah, Z. K., Layman, R., Jiang, X., and Gurcan, M. N. (2016). Quantification of liver fat: a comprehensive review. *Comput. Biol. Med.* 71, 174–189. doi: 10.1016/j.compbiomed.2016.02.013

Godin, A. C., Carlson, J. K., and Burgener, V. (2012). The effect of circle hooks on shark catchability and at-vessel mortality rates in longlines fisheries. *Bull. Mar. Sci.* 88, 469–483. doi: 10.5343/bms.2011.1054

Hirasaki, Y., Tomita, T., Yanagisawa, M., Ueda, K., Sato, K., and Okabe, M. (2018). Heart anatomy of *Rhincodon typus*: three dimensional x ray computed tomography of plastinated specimens. *Anatomical Rec.* 301, 1801–1808. doi: 10.1002/ar.23902

Hoyos-Padilla, E. M., Casanova-Santamaría, I., Loria-Correa, J. C., and Sulikowski, J. (2023). The successful use of a submersible ultrasound to confirm pregnancy on free swimming bull sharks, Carcharhinus leucas, in a provisioned shark site. *Front. Mar. Sci.* 10, 1193563. doi: 10.3389/fmars.2023.1193563

Huveneers, C., Meekan, M. G., Apps, K., Ferreira, L. C., Pannell, D., and Vianna, G. (2017). The economic value of shark-diving tourism in Australia. *Rev. Fish Biol. Fisheries* 27, 665–680. doi: 10.1007/s11160-017-9486-x

Joung, S.-J., Chen, C.-T., Clark, E., Uchida, S., and Huang, W. Y. (1996). The whale shark, *Rhincodon typus*, is a livebearer: 300 embryos found in one 'megamamma'supreme. *Environ. Biol. Fishes* 46, 219–223. doi: 10.1007/BF00004997

Ketchum, J. T., Galván-Magaña, F., and Klimley, A. P. (2013). Segregation and foraging ecology of whale sharks, *Rhincodon typus*, in the southwestern Gulf of California. *Environ. Biol. fishes* 96, 779–795. doi: 10.1007/s10641-012-0071-9

Kim, S. W., Yuen, A. H. L., Poon, C. T. C., Hwang, J. O., Lee, C. J., Oh, M.-K., et al. (2021). Cross-sectional anatomy, computed tomography, and magnetic resonance imaging of the banded houndshark (*Triakis scyllium*). *Sci. Rep.* 11, 1–15. doi: 10.1038/s41598-020-80823-y

Lai, N. C., Dalton, N., Lai, Y. Y., Kwong, C., Rasmussen, R., Holts, D., et al. (2004). A comparative echocardiographic assessment of ventricular function in five species of sharks. *Comp. Biochem. Physiol. Part A: Mol. Integr. Physiol.* 137, 505–521. doi: 10.1016/j.cbpb.2003.11.011

Matsumoto, R., Matsumoto, Y., Ueda, K., Suzuki, M., Asahina, K., and Sato, K. (2019). Sexual maturation in a male whale shark (*Rhincodon typus*) based on observations made over 20 years of captivity. *Fishery Bull.* 117, 78–86. doi: 10.7755/FB

Mattoon, J. S., Sellon, R. K., and Berry, C. R. (2020). *Small animal diagnostic ultrasound e-book* (Elsevier St Louis MO: Elsevier Health Sciences).

Mau, R. (2008). Managing for conservation and recreation: The Ningaloo whale shark experience. *J. Ecotourism* 7, 213–225. doi: 10.1080/14724040802140550

Mcclain, C. R., Balk, M. A., Benfield, M. C., Branch, T. A., Chen, C., Cosgrove, J., et al. (2015). Sizing ocean giants: patterns of intraspecific size variation in marine megafauna. *PeerJ* 3, e715. doi: 10.7717/peerj.715

Meekan, M., Austin, C. M., Tan, M. H., Wei, N.-W. V., Miller, A., Pierce, S. J., et al. (2017). iDNA at sea: recovery of whale shark (*Rhincodon typus*) mitochondrial DNA sequences from the whale shark copepod (*Pandarus rhincodonicus*) confirms global population structure. *Front. Mar. Sci.* 4, 420. doi: 10.3389/fmars.2017.00420

Meekan, M. G., Bradshaw, C. J., Press, M., Mclean, C., Richards, A., Quasnichka, S., et al. (2006). Population size and structure of whale sharks *Rhincodon typus* at Ningaloo Reef, Western Australia. *Mar. Ecol. Prog. Ser.* 319, 275–285. doi: 10.3354/meps319275

Meekan, M., Virtue, P., Marcus, L., Clements, K., Nichols, P., and Revill, A. (2022). The world's largest omnivore is a fish. *Ecology* 103, e3818. doi: 10.1002/ecy.3818

Meenakshisundaram, A., Thomas, L., Kennington, W. J., Thums, M., Lester, E., and Meekan, M. (2021). Genetic markers validate photo-identification and uniqueness of spot patterns in whale sharks. *Mar. Ecol. Prog. Ser.* 668, 177–183. doi: 10.3354/meps13729

Nijman, V. (2023). Illegal trade in protected sharks: The case of artisanal whale shark meat fisheries in Java, Indonesia. *Animals* 13, 2656. doi: 10.3390/ani13162656

Osorio, B. J., Skrzypek, G., and Meekan, M. (2023). Parasitic copepods as biochemical tracers of foraging patterns and dietary shifts in whale sharks (*Rhincodon typus* smith 1828). *Fishes* 8, 261. doi: 10.3390/fishes8050261

Penfold, L. M., and Wyffels, J. T. (2019). "Reproductive science in sharks and rays," in *Reproductive sciences in animal conservation*. Eds. P. Comizzoli, J. L. Brown and W. V. Holt (Cham Switzerland: Springer).

Pierce, S. J., Grace, M. K., and Araujo, G. (2021a). "Conservation of whale sharks," in *Whale sharks: biology, ecology, and conservation*. Eds. A. D. M. Dove and S. J. Pierce (CRC Press, Boca Raton, FL). doi: 10.1201/b22502

Pierce, S. J., and Norman, B. (2016). *Rhincodon typus*. The IUCN red list of threatened species 2016, e.19488A2365291. Available online at: http://www.iucnredlist.org/details/19488/0 (Accessed on June 5th, 2024).

Pierce, S. J., Pardo, S. A., Rohner, C. A., Matsumoto, R., Murakumo, K., Nozu, R., et al. (2021b). "Whale shark reproduction, growth, and demography," in *Whale sharks: biology, ecology, and conservation*. Eds. A. D. M. Dove and S. J. Pierce (CRC Press, Boca Raton, FL).

Reynolds, S. D., Redcliffe, J., Norman, B. M., Wilson, R. P., Holton, M., Franklin, C. E., et al. (2024). Swimming with humans: biotelemetry reveals effects of "gold standard" regulated tourism on whale sharks. *J. Sustain. Tourism.* 1–20. doi: 10.1080/09669582.2024.2314624

Rowat, D., Womersley, F., Norman, B. M., and Pierce, S. J. (2021). "Global threats to whale sharks," in *Whale sharks: biology, ecology, and conservation*. Eds. A. D. M. Dove and S. J. Pierce (CRC Press, Boca Raton, FL). doi: 10.1201/b22502

Sampaio, C. L., Leite, L., Reis-Filho, J. A., Loiola, M., Miranda, R. J., De Anchieta Cc Nunes, J., et al. (2018). New insights into whale shark *Rhincodon typus* diet in Brazil: an observation of ram filter-feeding on crab larvae and analysis of stomach contents from the first stranding in Bahia state. *Environ. Biol. fishes* 101, 1285–1293. doi: 10.1007/s10641-018-0775-6

Sequeira, A. M., Thums, M., Brooks, K., and Meekan, M. G. (2016). Error and bias in size estimates of whale sharks: implications for understanding demography. *R. Soc. Open Sci.* 3, 150668. doi: 10.1098/rsos.150668

Speed, C. W., Meekan, M. G., and Bradshaw, C. J. (2007). Spot the match–wildlife photo-identification using information theory. *Front. zoology* 4, 1–11. doi: 10.1186/1742-9994-4-2

Speed, C. W., Meekan, M. G., Rowat, D., Pierce, S., Marshall, A., and Bradshaw, C. J. (2008). Scarring patterns and relative mortality rates of Indian Ocean whale sharks. *J. Fish Biol.* 72, 1488–1503. doi: 10.1111/j.1095-8649.2008.01810.x

Speed, C. W., Meekan, M. G., Russell, B., and Bradshaw, C. J. (2009). Recent whale shark (*Rhincodon typus*) beach strandings in Australia. *Mar. Biodiversity Records* 2, e15. doi: 10.1017/S1755267208000158

Tait, R. G. (2016). Ultrasound use for body composition and carcass quality assessment in cattle and lambs. *Veterinary Clinics: Food Anim. Pract.* 32, 207–218. doi: 10.1016/j.cvfa.2015.09.007

Tomita, T., Murakumo, K., Ueda, K., Ashida, H., and Furuyama, R. (2019). Locomotion is not a privilege after birth: Ultrasound images of viviparous shark embryos swimming from one uterus to the other. *Ethology* 125, 122–126. doi: 10.1111/eth.12828

Walsh, M. T., Pipers, F. S., Brendemuehl, C. A., and Murru, F. L. (1993). Ultrasonography as a diagnostic tool in shark species. *Veterinary Radiol. Ultrasound* 34, 213–219. doi: 10.1111/j.1740-8261.1993.tb02008.x

Whitehead, D. A., Becerril-García, E. E., Petatán-Ramírez, D., Vázquez-Haikin, A., González-Armas, R., and Galván-Magaña, F. (2019). Whale shark *Rhincodon typus* strandings in the Gulf of California, Mexico. *J. fish Biol.* 94, 165–167. doi: 10.1111/jfb.13845

Womersley, F. C., Humphries, N. E., Queiroz, N., Vedor, M., Da Costa, I., Furtado, M., et al. (2022). Global collision-risk hotspots of marine traffic and the world's largest fish, the whale shark. *Proc. Natl. Acad. Sci.* 119, e2117440119. doi: 10.1073/pnas.2117440119

Wosnick, N., Leite, R. D., Giareta, E. P., Morick, D., and Musyl, M. (2022). Global assessment of shark strandings. *Fish Fisheries* 23, 786–799. doi: 10.1111/faf.12648

Yong, M. M. H., Leistenschneider, C., Miranda, J. A., Paler, M. K., Legaspi, C., Germanov, E., et al. (2021). Microplastics in fecal samples of whale sharks (*Rhincodon typus*) and from surface water in the Philippines. *Microplastics Nanoplastics* 1, 17. doi: 10.1186/s43591-021-00017-9

Yopak, K. E., and Lawrence, L. R. (2009). Brain size and brain organization of the whale shark, *Rhincodon typus*, using magnetic resonance imaging. *Brain Behav. Evol.* 74, i2i–i42. doi: 10.1159/000235962